

Self-absorption of synchrotron radiation in a laser-irradiated plasma

T. G. Blackburn,^{1,*} A. J. MacLeod,² A. Ilderton,² B. King,² S. Tang,² and M. Marklund¹

¹*Department of Physics, University of Gothenburg, SE-41296 Gothenburg, Sweden*

²*Centre for Mathematical Sciences, University of Plymouth,
Plymouth, PL4 8AA, United Kingdom*

(Dated: May 12, 2021)

Abstract

Electrons at the surface of a plasma that is irradiated by a laser with intensity in excess of 10^{23} Wcm⁻² are accelerated so strongly that they emit bursts of synchrotron radiation. Although the combination of high photon and electron density and electromagnetic field strength at the plasma surface makes particle-particle interactions possible, these interactions are usually neglected in simulations of the high-intensity regime. Here we demonstrate an implementation of two such processes: photon absorption and stimulated emission. We show that, for plasmas that are opaque to the laser light, photon absorption would cause complete depletion of the multi-keV region of the synchrotron photon spectrum, unless compensated by stimulated emission. Our results motivate further study of the density dependence of QED phenomena in strong electromagnetic fields.

* tom.blackburn@physics.gu.se

I. INTRODUCTION

Radiation emission from accelerated electrons is a ubiquitous feature of regions of strong electromagnetic field. In astrophysical environments [1], or in laser-matter interactions at the high-intensity frontier [2], the fields can be so strong that the interactions must be described within the framework of quantum electrodynamics (QED) [3–5]. Experiments at the next generation of high-intensity laser facilities [6–8] will produce high-energy γ rays via quantum synchrotron emission (also called nonlinear Compton scattering) in a variety of geometries [9–13]. Particle-in-cell (PIC) simulations, extended to include the one-particle to two-particle (‘1 to 2’) strong-field QED processes of photon emission and electron-positron pair creation [14, 15], play an essential role in modelling these interactions. However, for every emission process, there is a corresponding absorption process. To date, the inverse (‘2 to 1’) processes of one-photon absorption [16] and pair annihilation to one photon [17, 18] have been neglected in PIC simulations.

Here we consider the effect of one-photon absorption in a scenario where the photons are absorbed by the same population of relativistic electrons that emitted them. In an astrophysical context, this phenomenon is known as *synchrotron self-absorption* [19]. It leads to a steep cutoff at low frequency in the emission spectra from, e.g., supernovae [20], gamma-ray burst afterglows [21, 22], and black hole X-ray binaries [23]. In principle, the irradiation of a solid target by a laser of intensity $\gtrsim 10^{23} \text{ Wcm}^{-2}$ is a platform for studying self-absorption, because of the combination of strong electromagnetic field, high electron density, and high photon density at the plasma surface. A consistent treatment of photon absorption must include stimulated emission, which is the competing, induced process. To do so, we construct a cross section for stimulated emission in QED that is valid within the locally constant, crossed fields approximation; to the best of our knowledge, a cross section from QED has not previously been reported. We present an implementation of both as binary interactions between macroparticles in a PIC code. Simulating a laser-plasma interaction, we find that while photon absorption suppresses the multi-keV region of the synchrotron spectrum, this suppression is countered by stimulated emission. Our results demonstrate that it is feasible to include strong-field particle-particle interactions in studies of laser-driven plasmas.

II. INDUCED PROCESSES

The following master equation determines the evolution of the number of photons, $N(\mathbf{k})$, with momentum \mathbf{k} [24]:

$$\frac{dN(\mathbf{k})}{dt} = \int \frac{d^3\mathbf{p}}{(2\pi)^3} w(\mathbf{p}, \mathbf{k}) \{ [1 + N(\mathbf{k})] f(\mathbf{p}) - N(\mathbf{k}) f(\mathbf{p} - \mathbf{k}) \}. \quad (1)$$

Here $w(\mathbf{p}, \mathbf{k})$ is the rate at which an electron with momentum \mathbf{p} emits photons with momentum \mathbf{k} and $f(\mathbf{p})$ is the electron distribution function, defined by $dN_e = f(\mathbf{p}) d^3\mathbf{p}/(2\pi)^3$. (We use units such that $\hbar = c = 1$ throughout). The first term in square brackets on the RHS of eq. (1) describes ‘spontaneous emission’, which is the quantum synchrotron emission already included in laser-plasma simulations [14, 15]. The following two terms correspond, respectively, to the induced processes of stimulated emission and photon absorption. Unlike spontaneous emission, they depend on the density of photons already present. All three processes depend on the electron and photon momenta, p^μ and k^μ , and the strength of the electromagnetic field $F_{\mu\nu}$, which is implicit in $w(\mathbf{p}, \mathbf{k})$. Stimulated emission does not represent an interaction in the same sense that absorption does: a photon is not absorbed and re-emitted, for example. It is a consequence of the fact that photons are bosons, which means that the phase space for the emission of a photon with momentum \mathbf{k} is enhanced by the presence of photons with the same momentum. (For fermions, the equivalent phenomenon, Pauli blocking, would be de-enhancing.)

Conservation of momentum means that an electron in vacuum cannot absorb radiation without some associated emission of radiation. Absorption can occur, however, for an electron in a background electromagnetic field $F_{\mu\nu}$ (where the required emissions appear as ‘absorption’ of negative frequency modes from the background [16]). If the field is weak compared to the critical field of QED, $E_{\text{cr}} = m^2/e$ [25, 26], and if it varies sufficiently slowly such that quantum processes can be considered to be instantaneously constant, the interaction is controlled by the quantum parameters $\chi_e = |F_{\mu\nu} p^\nu|/(mE_{\text{cr}})$ and $\chi_\gamma = |F_{\mu\nu} k^\nu|/(mE_{\text{cr}})$, where p and k are the electron and photon momenta, e is the elementary charge and m is the electron mass.

We may derive cross sections for absorption and stimulated emission from the master equation, eq. (1), as follows. Consider a monoenergetic electron population, such that $f(\mathbf{p}') = N_e \delta(\mathbf{p}' - \mathbf{p})$. The last term in eq. (1) is the absorption contribution:

$$\left. \frac{dN(\mathbf{k})}{dt} \right|_{\text{abs}} = -N_e w(\mathbf{p} + \mathbf{k}, \mathbf{k}) N(\mathbf{k}) = -4\pi^3 n_e \frac{dW(\mathbf{p} + \mathbf{k})}{d^3\mathbf{k}} N(\mathbf{k}), \quad (2)$$

where we have used $w(\mathbf{p}, \mathbf{k}) = \frac{(2\pi)^3}{2V} \frac{dW}{d^3\mathbf{k}}$ and absorbed the volume factor V into the electron number density, $n_e = N_e/V$. If the background field is constant and crossed, the triple-differential photon emission rate $\frac{dW}{d^3\mathbf{k}}$ is given by [27]:

$$\frac{dW(\mathbf{p})}{d^3\mathbf{k}} = \frac{\alpha}{\sqrt{3}\pi^2 m^2} \frac{\zeta^{1/3}(1+u)}{\gamma^2 \chi_e u} \left\{ \zeta^{2/3} [1 + (1+u)^2] - (1+u) \right\} K_{1/3} \left(\frac{2u\zeta}{3\chi_e} \right), \quad (3)$$

where

$$u = \frac{\omega}{\gamma m - \omega} = \frac{s}{1-s}, \quad \zeta = [2\gamma^2(1 - \beta \cos \theta)]^{3/2} = \left(\frac{2k \cdot p}{s m^2} \right)^{3/2}. \quad (4)$$

Here ω is the photon energy, γ is the Lorentz factor of an electron with velocity β , and θ is the angle between the electron and photon momentum (assumed to be small in the ultrarelativistic limit $\gamma \gg 1$). The rate at which photons are absorbed depends on the synchrotron emissivity of an electron with momentum $\mathbf{p} + \mathbf{k}$ [28]. In order to obtain an equivalent of eq. (3) for an electron with momentum $\mathbf{p}' = \mathbf{p} + \mathbf{k}$, we make the following substitutions: $u \rightarrow s$, $\gamma \rightarrow \gamma(1+s)$, $\chi_e \rightarrow \chi_e(1+s)$. The parameter ζ is *not* changed. This may be seen by calculating $k \cdot p'$ in terms of $k \cdot p$, and applying the conservation of momentum in a crossed field with lightlike wavevector n : $p + k = p' + [k \cdot p/n \cdot (k + p)]n$. Dividing eq. (2) by another volume factor V , to obtain a photon number density n_γ , gives us the number of absorption events per unit volume, per unit time:

$$-\left. \frac{dn_\gamma}{dt} \right|_{\text{abs}} = 4\pi^3 n_e n_\gamma \frac{dW(\mathbf{p} + \mathbf{k})}{d^3\mathbf{k}} = \underbrace{\frac{n_e n_\gamma k \cdot p}{s\gamma^2 m^2}}_{\text{invariant flux}} \underbrace{\frac{4\pi^2 \alpha}{k \cdot p} \frac{4g\bar{z} - z}{s}}_{\text{cross section}} \text{Ai}(\bar{z}), \quad (5)$$

where we identify the final result as the product of the invariant flux $F = n_e n_\gamma k \cdot p / (k^0 p^0)$ and a cross section σ . The auxiliary variables are $s = \chi_\gamma / \chi_e$, $g = \frac{1}{2} + \frac{s^2}{4(1+s)}$, $z = \{s / [\chi_e(1+s)]\}^{2/3}$ and $\bar{z} = (2z/s)(k \cdot p/m^2)$.

A similar logic may be followed to obtain the cross section for stimulated synchrotron emission. From the second term in eq. (1),

$$\left. \frac{dN(\mathbf{k})}{dt} \right|_{\text{st}} = N_e w(\mathbf{p}, \mathbf{k}) N(\mathbf{k}) = 4\pi^3 n_e \frac{dW(\mathbf{p})}{d^3\mathbf{k}} N(\mathbf{k}), \quad (6)$$

we obtain

$$\left. \frac{dn_\gamma}{dt} \right|_{\text{st}} = \underbrace{\frac{n_e n_\gamma k \cdot p}{s\gamma^2 m^2}}_{\text{invariant flux}} \underbrace{\frac{4\pi^2 \alpha}{k \cdot p} \frac{4g'\bar{z}' - z'}{s}}_{\text{cross section}} \text{Ai}(\bar{z}'), \quad (7)$$

where $s = \chi_\gamma / \chi_e$, $g' = \frac{1}{2} + \frac{s^2}{4(1-s)}$, $z' = \{s / [\chi_e(1-s)]\}^{2/3}$ and $\bar{z}' = (2z'/s)(k \cdot p/m^2)$. Note that the same \mathbf{k} appears on both sides of eq. (6) and therefore, when stimulated emission occurs, the emitted and stimulating photons have the same momentum.

The cross sections for absorption and stimulated emission may therefore be written in a unified form, as:

$$\sigma = \frac{4\pi^2\alpha}{k.p} \frac{z(4g\bar{z}/z - 1) \text{Ai}(\bar{z})}{s}, \quad (8)$$

where $s = \chi_\gamma/\chi_e$ and $\bar{z} = (2z/s)(k.p/m^2)$ for both processes. In the remaining two auxiliary variables, $g = 1/2 + s^2/[4(1 \pm s)]$ and $z = \{s/[\chi_e(1 \pm s)]\}^{2/3}$, choosing the positive (negative) sign yields the cross section for absorption (stimulated emission). The sign of s in the definitions of g and z is an expression of the conservation of momentum. An electron may absorb a photon with arbitrarily large energy and therefore s may take any value. However, stimulated emission can only take place for photons with *less* energy than the electron; thus on kinematic grounds, we have the restriction $s < 1$. The cross section for absorption, obtained in this way, agrees with the result of a direct calculation from strong-field QED [16], which is a useful crosscheck of the master equation approach. To the best of our knowledge, a QED cross section for stimulated emission has not previously been reported.

This result is obtained in the locally constant, crossed field approximation (LCFA), under which the rate for a QED process in an arbitrary background field may be replaced with its equivalent in a constant, crossed field [29]. The validity of this approximation depends on the normalized field amplitude $a_0 = eE_0/(m\omega_0)$, where E_0 is the electric field strength and ω_0 is the field's frequency of oscillation. The LCFA holds for the '1 to 2' processes of Compton scattering [30–34] and nonlinear Breit-Wheeler pair creation [35] if a_0 satisfies $a_0 \gg 1$ and $a_0^3/\chi_{e,\gamma} \gg 1$, as under these conditions the formation length is much smaller than the scale of variation of the background field. In a pulsed background, however, there are always temporal regions where the local value of a_0 is small, and hence the assumptions of the LCFA are automatically violated. Compton scattering and Breit-Wheeler pair creation 'self-regulate' in this situation [34]; while the fractional error in the rate is large in such regions, the rate itself is small (in fact, vanishing) due to the behaviour of the Airy functions appearing there, and thus the absolute error is small. The question arises as to what extent these statements apply also to induced processes, which depend on additional kinematic variables.

A comparison of the LCFA for one-photon absorption eq. (8) with the full QED result [16] in a monochromatic plane-wave background shows good agreement for $s \gtrsim \chi_e/a_0^3$. Absorption is, though, more likely in regions where a_0 is not large. In very short pulses, these regions can contribute a significant proportion of the total probability [16]. However, note that [16] benchmarked

absorption using externally injected photons, which overlap with the electrons even in free space. Here we consider photons that are emitted by the electron population itself, so that overlap takes place only in the high-field region, $a_0 \gg 1$, where emission is most likely. As the LCFA is satisfied for the emission process in this regime, and emission and absorption take place in the same region of space, it should also be satisfied for the absorption process.

Emission of a photon by an electron, followed by absorption of that photon by another electron, may be viewed as the component of Møller scattering ($ee \rightarrow ee$, in a strong field) in which the intermediate photon is real. A complete treatment of electron-electron scattering in a background field would include off-shell and interference contributions; this has been done for monochromatic [36–39] and pulsed electromagnetic waves [40] at low intensity $a_0 \lesssim 1$, with particular focus on resonances in the transition amplitude. These resonances occur when the intermediate photon goes on shell, which significantly enhances the interaction probability over its value in vacuum. This is precisely the interaction under consideration here. It should dominate the virtual component, i.e. direct electron-electron scattering, which is, in its usual classical description [41], negligible for laser-plasmas.

III. IN A LASER-PLASMA ENVIRONMENT

A. Analytical estimates

Let us first determine the laser and plasma parameters for which one-photon absorption becomes important. Consider a population of electrons, with number density n_e , performing a circular orbit with Lorentz factor γ , quantum parameter χ_e and gyroradius $R_c = \gamma^2/(m\chi_e)$. Let the space be filled by photons with number density n_γ , quantum parameter χ_γ and energy ω , all propagating in the same direction and in the plane of the electron orbit.

Defining θ to be the angle between the electron and photon momenta and assuming $\gamma \gg 1$ and $\theta \ll 1$, the argument of the Airy function in eq. (8) may be cast as $\bar{z} \simeq \theta^2/\theta_c^2$, for $\theta_c = [m\chi_e/(\gamma^2\omega)]^{1/3}$. This shows that the cross section is suppressed for $\theta > \theta_c$, i.e. unless the electron and photon are almost collinear, so it occurs once per orbit. In general, both absorption and stimulated emission are likeliest for low-energy photons propagating at small angles to the electron trajectory.

The number of events per unit volume $n_{\text{abs}} = \int F \sigma(t) dt$, where $F = n_e n_\gamma k \cdot p / (k^0 p^0)$ is the

invariant flux, $\sigma(t)$ the instantaneous cross section, and the integral is taken over the interval where \mathbf{p} is close to parallel with \mathbf{k} . Assuming that $s = \chi_\gamma/\chi_e \ll 1$ and the angle between electron and photon $\theta(t) = t/R_c \ll 1$, we obtain

$$F\sigma(t) = \frac{4\pi^2\alpha n_e n_\gamma}{m^2} \frac{1+2\gamma^2\theta^2}{\gamma^2\chi_e^{2/3}s^{4/3}} \text{Ai}\left[(s/\chi_e)^{2/3}(1+\gamma^2\theta^2)\right]. \quad (9)$$

We integrate eq. (9) using the fact that

$$\int_{-\infty}^{\infty} (1+2\tau^2) \text{Ai}[\xi(1+\tau^2)] d\tau \simeq 0.530\xi^{-3/2} \quad (10)$$

for $\xi \ll 1$. The fraction of photons absorbed by the electrons is given by:

$$f_{\text{abs}} = \frac{n_{\text{abs}}}{n_\gamma} \simeq \frac{0.15n_e}{m^3\gamma\chi_e^{2/3}s^{7/3}}. \quad (11)$$

In the case that the electrons are in a plasma that is driven by a circularly polarized laser with angular frequency ω_0 , we can set $\chi_e = \gamma^2\omega_0/m$ and express the density n_e in terms of the critical density $n_{\text{cr}} = m\omega_0^2/(4\pi\alpha)$. We define the self-absorption frequency ω_{abs} as the largest frequency for which the absorption fraction $f_{\text{abs}} \gtrsim 1$:

$$\omega_{\text{abs}}[\text{keV}] \simeq 0.4 \left(\frac{n_e}{n_{\text{cr}}}\right)^{3/7} \lambda^{-4/7}[\mu\text{m}] \quad (12)$$

Photons with energies smaller than ω_{abs} , which lies in the multi-keV range for overdense plasmas, should be efficiently absorbed.

The probability that scattering, via the linear Compton process $e\gamma \rightarrow e\gamma$, occurs instead of absorption is negligible for photons satisfying eq. (12). The fraction of photons scattered $f_{\text{sc}} = \int F\sigma_{\text{sc}}dt$, where $F = n_e n_\gamma k \cdot p / (k^0 p^0) \simeq n_e n_\gamma (1 - \cos\theta)$ is the invariant flux and we take $\sigma_{\text{sc}} = 8\pi\alpha^2/(3m^2)$ as a representative value of the Compton cross section. The integral over a single orbit yields $f_{\text{sc}}/f_{\text{abs}} \simeq 0.019s^{7/3}\gamma^3/\chi_e^{1/3}$: for electrons in a plasma driven by a circularly polarized laser, this is equivalent to $f_{\text{sc}}/f_{\text{abs}} \simeq 6.7 \times 10^{-7} \omega^{7/3}[\text{keV}]\lambda^{1/3}[\mu\text{m}]$. Under these circumstances, it is safe to neglect scattering for the multi-keV photons that are of interest here.

Note that there is no dependence on laser intensity in eq. (12). The laser intensity does, however, play a role, in that the origin of the photons that are to be absorbed is electron synchrotron radiation, which only becomes substantial if the laser intensity is sufficiently high [10–12]. We now estimate the properties of this emission for the scenario of a laser-irradiated, overdense plasma. Only electrons within the skin layer are exposed to strong electromagnetic fields; the

effective value of the laser amplitude is reduced by screening from a_0 , its value in vacuum, to $a_{\text{eff}} \simeq a_0 \sqrt{n_{\text{cr}}/n_e}$ [10]. (This result strictly applies only in the nonrelativistic limit [42], but it is consistent with the simulation results to be presented.)

Electrons are accelerated on segments of circular trajectories, with Lorentz factor $\gamma \simeq a_{\text{eff}}$, and emit synchrotron radiation with a characteristic frequency of $\omega_{\text{cr}} \simeq \gamma^3 \omega_0$. We expect the LCFA to be valid for the emission and absorption of photons that satisfy $s > \chi_e/a_0^3$, which is equivalent to $\omega > \omega_0$. This is satisfied for both the self-absorption frequency ω_{abs} and the characteristic frequency of emission ω_{cr} : with $n_e = 100n_{\text{cr}}$ and $a_0 = 400$, for example, $\gamma \simeq a_{\text{eff}} \simeq 40$, $\chi_e = \gamma^2 \omega_0/m \simeq 5 \times 10^{-3}$ and $\omega_{\text{cr}} \simeq 100$ keV. The treatment of synchrotron radiation as incoherent requires that the frequencies of interest $\omega > \omega_{\text{coh}}$, where $\omega_{\text{coh}} = n_e^{1/3}$ is an upper limit for the onset of coherence effects [15]. Both ω_{abs} and ω_{cr} meet this requirement by at least a factor of two.

The cross sections for stimulated emission and absorption are similar in magnitude for $s \ll 1$ [28]. The balance between the two is determined by the gradient in momentum space of the electron distribution function: net absorption occurs when this is negative, i.e. there are more electrons at lower energy than at higher energy [24]. This dependence on the electron distribution function means that we turn to numerical methods, i.e. particle-in-cell simulations.

B. Implementation in numerical simulations

Particle-in-cell simulations now incorporate both the quantum emission and absorption of synchrotron radiation, in addition to classical, relativistic plasma dynamics. In this work, emission is modelled in the usual Monte Carlo approach [14, 15] by integrating the LCFA rate [3, 29] along the electron trajectory and sampling the quantum synchrotron spectrum. We use a spectrum that is differential in both energy and scattering angle [27, 43]. Absorption and stimulated emission are incorporated as a binary interaction between macroparticles.

The probabilities of absorption and stimulated emission for an individual macrophton (index i) are controlled by two optical depths τ_i^ℓ ($\ell = \text{abs}, \text{stim}$). To ensure correct statistics, these are initialized with exponentially distributed values, i.e. $\tau_i^\ell = -\ln U_i^\ell$, where the U_i^ℓ are pseudorandom numbers chosen on the unit interval [14]. At every timestep, the interaction probability P_{ij}^ℓ is calculated for all pairwise combinations of macroelectrons j and macrophtons i that are located in the same grid cell, using the cross sections given in eq. (8): $P_{ij}^\ell = w_j (c\Delta t/V) (k_i \cdot p_j / k_i^0 p_j^0) \sigma^\ell$, where w_j is the macroelectron weight, Δt is the timestep, V is the volume of a grid cell, k is the

four-momentum of the photon, and p is the four-momentum of the electron. Each interaction therefore corresponds to a single absorption (emission) event, rather than to a cumulative treatment of scattering often used for Coulomb collisions [44, 45]; a similar scheme has been used to implement linear Compton scattering in PIC simulations [46].

While the cross sections eq. (8) are derived for a plane electromagnetic wave in the constant field limit, it is applied to arbitrary background fields in our code. To do so, we replace $s \rightarrow k^0/p^0$ in the factor of \bar{z}/z appearing in the prefactor. (Elsewhere it remains $s = \chi_\gamma/\chi_e$.) The purpose of this change is to guarantee that the cross section is positive. We have verified that it does not change the final results of our simulations, as eq. (8) is strongly suppressed unless the electron and photon are almost collinear.

The macrophoton's optical depths are updated as $\tau_i^\ell \rightarrow \tau_i^\ell - P_{ij}^\ell$ for each electron (index j), until one of τ_i^ℓ falls below zero. The relevant interaction is then deemed to occur; in combination with the initialization of τ_i^ℓ described above, this ensures the correct distribution of scattering events [14]. If absorption occurs ($\tau_i^{\text{abs}} < 0$), the macroelectron momentum is updated as $\mathbf{p}_j \rightarrow \mathbf{p}_j + w_i \mathbf{k}_i / w_j$, where w_i is the weight of the macrophoton, and the macrophoton is deleted from the simulation. (The weight factors appear in order to ensure conservation of momentum.) If stimulated emission occurs ($\tau_i^{\text{stim}} < 0$), the macroelectron momentum is updated as $\mathbf{p}_j \rightarrow \mathbf{p}_j - \mathbf{k}_i$, a new macrophoton with momentum \mathbf{k}_i and weight w_j is added to the simulation, and the optical depth of the stimulating photon τ_j^{stim} is reinitialized. Should both optical depths fall below zero simultaneously, a pseudorandom number U' is drawn on the unit interval and absorption selected if $U' < P_{ij}^{\text{abs}} / (P_{ij}^{\text{abs}} + P_{ij}^{\text{stim}})$; otherwise stimulated emission is selected. Benchmarking against analytical results are given in appendix A.

C. Results

As an example, we simulate the interaction of a 10-fs (fwhm duration), circularly polarized laser pulse with a slab of fully ionized carbon plasma, density $n_e = 100n_{\text{cr}}$ and thickness 5.0 μm , at normal incidence. The laser amplitude is $a_0 = 400$ and its wavelength $\lambda = 800$ nm, which yields an electron density of $1.7 \times 10^{23} \text{ cm}^{-3}$. The simulation is performed in 1D, with 1000 cells per micron and 200 particles per cell for each species. This neglects the possibility that electrons and photons escape the laser focal spot in one of the transverse directions, as these are ignored in 1D. However, we show that photons are absorbed (or stimulate emission) in a sufficiently short

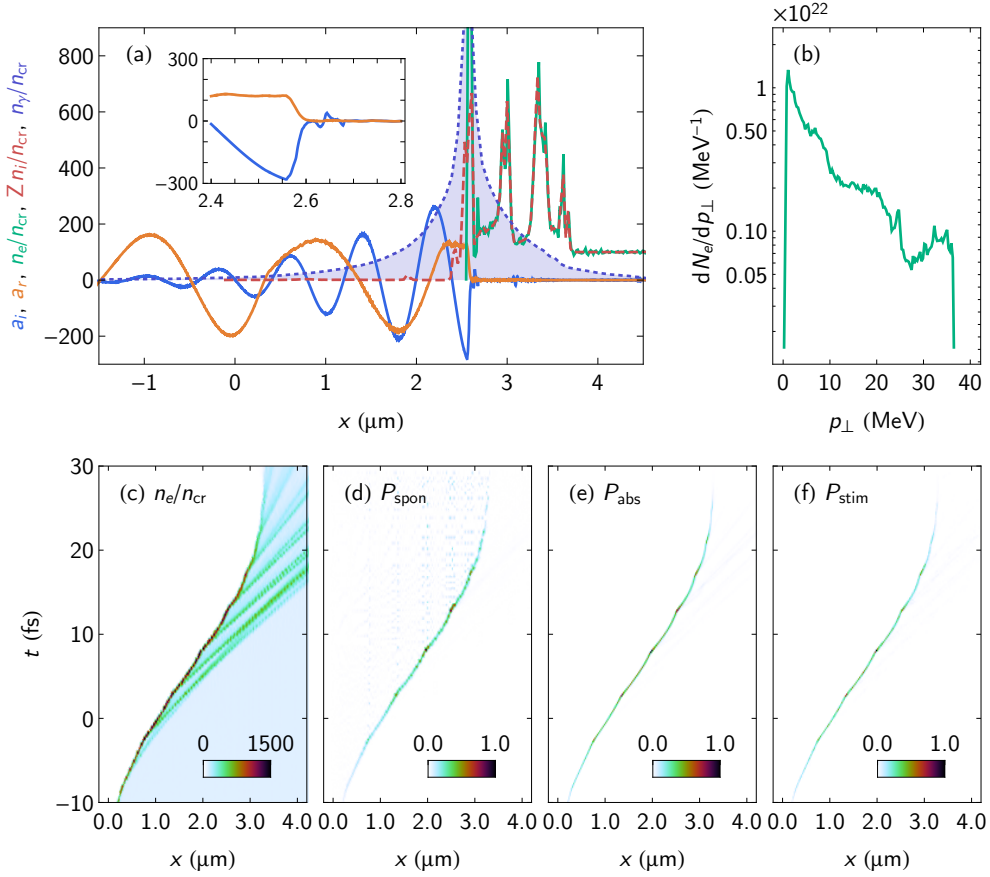


FIG. 1. (a) The normalized incident and reflected electromagnetic fields (blue and orange) and electron (green), ion (red, dashed) and photon (purple, dashed) number densities at $t = 13.3$ fs. (b) Perpendicular momentum distribution of electrons located at positions $x \leq 2.6$ μm , i.e. within the skin layer, at $t = 13.3$ fs. (c) The electron number density as a function of time t and longitudinal coordinate x . (d) The probability density that a photon is emitted (spontaneously) at time t and position x . (e) The probability density that a photon, if absorbed, is absorbed at time t and position x . (f) The probability density that photon emission is stimulated at time t and position x . In (d-f) all probability densities are normalized to their maxima.

timescale after emission that the perpendicular distance travelled is small. Simulations include radiation emission (both spontaneous and stimulated) and absorption by the method discussed in section III B. The validity of the LCFA in this scenario, upon which this method depends, is discussed in appendix B. Binary interactions between electrons or photons and ions, such as bremsstrahlung, are suppressed as carbon has a relatively small atomic number $Z = 6$; as discussed in section III A, linear Compton scattering is negligible.

The y components of the incident and reflected electromagnetic field, as well as the electron, ion and photon number densities at $t = 13.3$ fs are shown in fig. 1(a). (Time $t = 0$ corresponds to the centre of the laser pulse crossing $x = 0$, the location of the unperturbed vacuum interface.) Electrons near the plasma surface are accelerated on circular orbits by the laser fields, with perpendicular momenta $p_{\perp} \simeq ma_{\text{eff}}$, as shown in fig. 1(b), and displaced by the radiation pressure in the x -direction, as shown in fig. 1(c). This establishes a charge-separation field that accelerates the ions in turn. In the steady state, the velocity of the hole-boring front is $\beta_{\text{hb}} = \sqrt{\Xi}/(1 + \sqrt{\Xi})$, where $\Xi = Zn_{\text{cr}}ma_0^2/(An_em_p)$ [47], Z and A are the atomic and mass numbers of the ion species, and m_p is the proton mass. For the parameters under consideration here, $\beta_{\text{hb}} \simeq 0.40$, which is consistent with simulation results.

In order to identify when and where induced processes occur, we use the simulation data to calculate the probability density $p(t, x)$ that a photon, if it undergoes absorption or stimulated emission, does so at time t and coordinate x . These two probability densities, along with the equivalent for spontaneous synchrotron emission, are shown in fig. 1(d-f): as all three have unit integral, $\iint p(t, x) dt dx = 1$, they are scaled by their respective maxima. Figure 1(d) shows that synchrotron radiation originates from electrons in the skin layer, close to the hole-boring front, where the laser fields are only partially screened. The skin layer is also where photon absorption and stimulated emission take place [see fig. 1(e) and (f)], because the photons and electrons are only aligned within an angle of $1/\gamma$ shortly after emission, the local densities are high, and screening of the background field is not complete. By recording the time of emission for each photon, as well the momentum, we may calculate the total distance travelled before absorption occurs (including in the transverse directions). Of all the photons that are absorbed, 90% are absorbed before they have propagated a distance of 10 nm. The smallness of this distance, as compared to the typical size of a laser focal spot, indicates multidimensional effects can safely be neglected. If the radiation escapes the skin layer, it is highly unlikely to be absorbed thereafter.

The radiation spectrum at the end of the simulation, when the plasma is no longer driven by the laser, is shown in fig. 2. As emission takes place when the electron momentum is instantaneously perpendicular to the laser fields, in the rest frame of the plasma surface, we expect the synchrotron radiation to appear predominantly at polar angles θ satisfying $\cos \theta \simeq \beta_{\text{hb}}$, where β_{hb} is the hole-boring velocity. This is confirmed by fig. 2(b) and (c), which show the radiation spectrum as a function of energy and polar angle. ($\theta = 0$ corresponds to forward emission, i.e. parallel to the laser wavevector.)

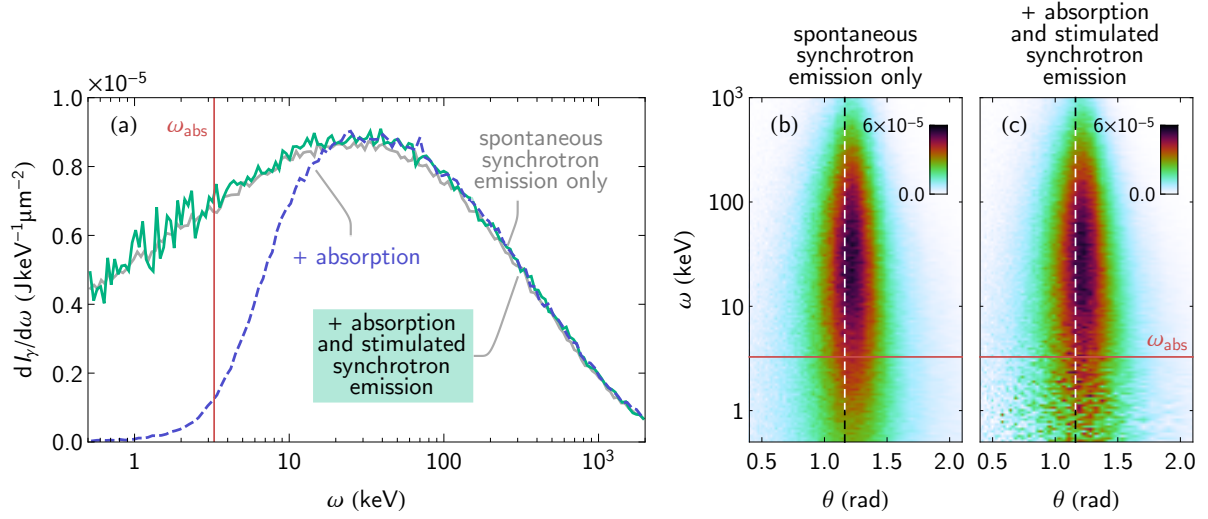


FIG. 2. Spectra of the synchrotron photons emitted when plasma with density $n_e = 100n_{\text{cr}}$ is irradiated by a circularly polarized laser with peak amplitude $a_0 = 400$: (a) energy radiated per unit frequency, per unit area illuminated, at polar angles $65^\circ < \theta < 75^\circ$ to the laser axis; (b, c) as in (a), but differential in the polar angle, rather than integrated over it. Solid red lines give ω_{abs} , eq. (12), our theoretical prediction for the onset of absorption. Dashed lines give $\cos \theta \simeq \beta_{\text{hb}}$, the expected emission angle from a surface moving at the hole-boring velocity β_{hb} .

There is a significant reduction in the number of multi-keV photons when one-photon absorption is taken into account. The threshold energy at which the spectrum is suppressed is consistent with our theoretical estimate eq. (12), substituting $n_e/n_{\text{cr}} = 100$. However, this suppression is countered by stimulated emission, leading to a photon spectrum that is almost identical to the ‘spontaneous emission only’ result. This also applies to the angularly resolved spectra, shown in fig. 2(b) and (c), with the caveat that there is increased statistical noise in the latter. This arises because, when both absorption and stimulated emission are included, the photon distribution function is effectively resampled at every timestep. In astrophysical scenarios, it is expected that net absorption causes the spectrum to be suppressed as $\omega^{5/2}$ at $\omega \ll \omega_{\text{cr}}$ [22], assuming that the electron population has a power-law distribution of energies $dN_e/d\gamma \propto \gamma^{-p}$ ($p > 0$) and that each electron emits and absorbs at a single frequency $\omega_{\text{cr}}(\gamma)$. This is not observed here, as the electron perpendicular momentum distribution shown in fig. 1(b), while having negative gradient, is not sufficiently broad. We expect that similar results would be obtained for a linearly polarized laser, albeit that there would be significantly more synchrotron radiation in the MeV energy range due

to increased electron heating. Absorption and stimulated emission of photons will still occur at the hole-boring front, where the particle density is high and where the electrons and photons are momentarily aligned.

IV. CONCLUSIONS

In this paper we have considered the interplay between the standard strong-field QED process of nonlinear Compton scattering, or spontaneous photon emission, and the particle-particle processes of absorption and stimulated emission. By constructing cross sections for these processes within the same scheme (based on the locally constant field approximation) used for spontaneous emission, we have shown that it is feasible to include induced, particle-particle processes in simulations of laser-plasma interactions. This allows us to capture phenomena that are primarily dependent on density. While photon absorption occurs prolifically for multi-keV synchrotron photons in a laser-plasma interaction, *net* absorption is weak because of stimulated emission. Our results motivate investigation into the density dependence of QED phenomena in strong fields, which adds a new axis to the standard parameter space of intensity (a_0) and energy ($\chi_{e,\gamma}$).

ACKNOWLEDGMENTS

We are very grateful to John Kirk for helpful discussions during the preparation of this work. We acknowledge funding from the Swedish Research Council (grant 2016-03329, M.M.) and the Engineering and Physical Sciences Research Council (grant EP/S010319/1, A.I., B.K., A.J.M., S.T.). Simulations were performed on resources provided by the Swedish National Infrastructure for Computing at the High Performance Computing Centre North and National Supercomputer Centre.

DATA AVAILABILITY

The source code for the PIC simulations is available at Ref. [48]. Version 1.5.1, used in this work, and the data necessary to reproduce the simulation results are openly available at Ref. [49].

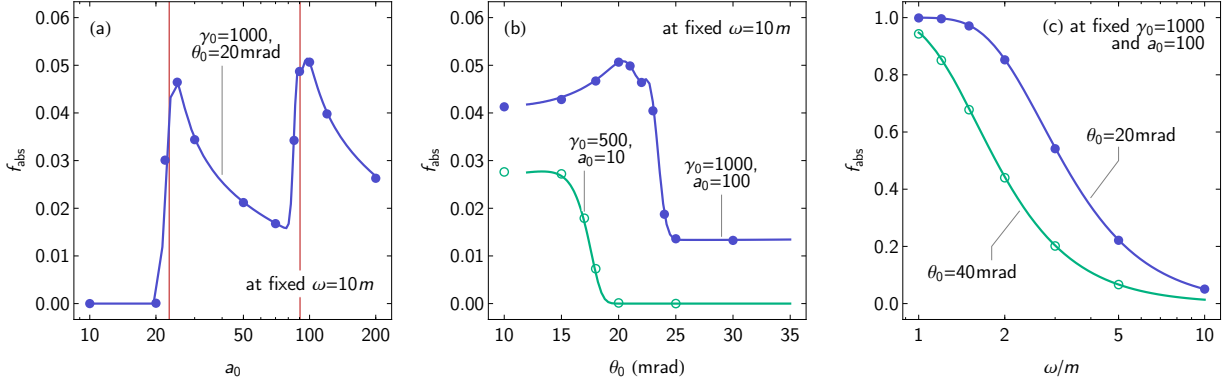


FIG. 3. Benchmarking of the PIC implementation (points) against analytical predictions (solid lines) for the fraction of photons absorbed f_{abs} , as a function of (a) laser amplitude a_0 , (b) collision angle θ_0 and (c) photon energy ω . The red vertical lines in (a) indicate the matching conditions $\gamma_0 \theta_0 / a_0 = 0.211$ and 0.870 , where the electron and photon beams are parallel at the field maxima of the laser pulse. The initial electron and photon densities are $n_e = n_\gamma = 10^{34} \text{ m}^{-3}$.

Appendix A: Benchmarking

To ensure that the PIC implementation of one-photon absorption outlined in section III B is accurate, we benchmark against the analytical cross section derived in [16], for absorption. We consider a linearly polarized plane wave pulse with a \cos^2 -envelope of duration $\tau \sim 7$ fs, normalized amplitude a_0 and wavelength $\lambda_0 = 0.8 \text{ } \mu\text{m}$. The potential is given by $eA(\phi) = ma_0 \sin(\phi) \cos^2(\pi\phi/L)$ for phases $|\phi| < L/2$, where $L = 4\pi$. A beam of electrons, with initial energy $\gamma_0 m$ and density n_e , and a beam of photons, with energy ω and density n_γ , are injected into this pulse: the electron beam counterpropagates into the laser pulse, and we vary the initial angle between the photon beam and laser wavevector θ_0 . ($\theta_0 = 0$ corresponds to the electron and photon beams being initially parallel to one another, i.e. both counterpropagating to the laser.) Each beam is modelled with 200 macroparticles per cell; we have also verified that varying the number of macroelectrons and macrophotons per cell from (400, 200), to (200, 200), and then to (200, 400), does not alter the results.

A suitable observable is the fraction, f_{abs} , of photons absorbed from the initial beam. Analytically, this is given by

$$f_{\text{abs}} = 1 - \exp\left(-n_e \sigma_{\text{int}} \tau \frac{1 - \cos \theta_0}{1 + \cos \theta_0}\right), \quad (\text{A1})$$

where $\sigma_{\text{int}} = \frac{1}{L} \int_{-L/2}^{L/2} \sigma(\phi) d\phi$ is the integrated cross section (Eq. 32 in [16]) and $\tau = L/\omega_0$ is the laser duration. In fig. 3 we compare the fraction of absorbed photons eq. (A1) using σ_{int} calculated analytically from [16], with that obtained numerically by the PIC simulations outlined in section III B. To ensure a fair comparison, photon emission (both spontaneous and stimulated) and current deposition are disabled in the simulations.

The results of our PIC implementation (points) show excellent agreement with the analytical predictions (solid lines) over parameter scans in the field strength a_0 , initial photon beam angle θ_0 , and energy ω . In particular, the PIC implementation correctly resolves the peak structure seen in the dependence of the absorbed fraction f_{abs} on the field strength a_0 . These peaks arise when the electrons and photons are brought into alignment at a local maximum of the field amplitude, i.e., when the instantaneous angle between the electron momentum and the laser wavevector, $\theta_e(\phi) \simeq eA(\phi)/(m\gamma_0)$, satisfies $\theta_e(\phi) = \theta_0$, at a phase ϕ where $\partial_\phi A(\phi) = 0$. For the two-cycle pulse under consideration here, the matching condition is $\gamma_0 \theta_0/a_0 = 0.211$ and 0.870 .

The densities employed to generate fig. 3, $n_e = n_\gamma = 10^{34} \text{m}^{-3}$, are sufficiently high that ignoring current deposition is unphysical. However, as discussed in the main text above, one can alleviate this problem by considering the absorption of synchrotron photons generated in the hole-boring regime. The simulations discussed in the main text do include the fields generated by the plasma.

Appendix B: Finite formation length effects

In section III C, we present PIC simulations of a laser-plasma interaction, which include spontaneous and stimulated synchrotron emission, as well as absorption. The rates (cross sections) for these processes are calculated within the locally constant field approximation (LCFA). Physically, this requires that the photon ‘formation length’, the characteristic distance over which emission takes place, be smaller than the spatial scale of variation of the external electromagnetic field [29]. The failure of the LCFA at small photon energies or low intensity has motivated a search for photon emission rates that are valid for non-constant backgrounds and appropriate for inclusion in simulations: various methods are now available [32, 34].

In this section we estimate the error made by our simulations in using the LCFA, by means of the method described in [43]. This exploits the fact that the LCFA photon emission rate sampled by the code is differential in both energy and angle. Consequently, the formation length L_f may be estimated as the distance travelled by the electron before it is deflected by an angle ϑ , where ϑ

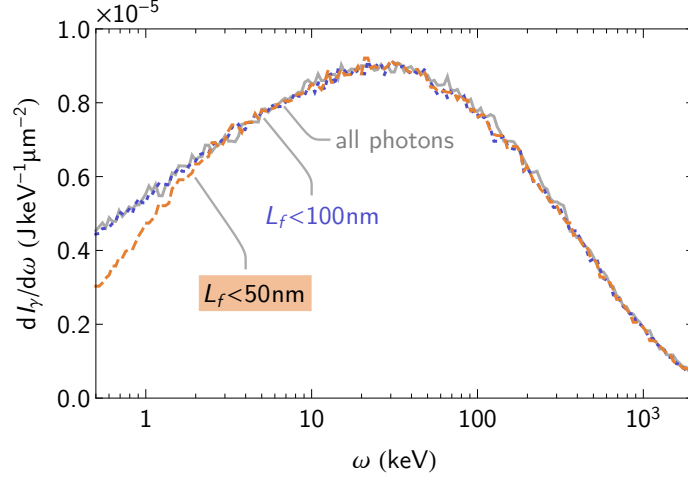


FIG. 4. Spectra of the synchrotron photons emitted when plasma with density $n_e = 100n_{\text{cr}}$ is irradiated by a circularly polarized laser with peak amplitude $a_0 = 400$, as shown in fig. 2: all photons (grey), photons with formation lengths L_f smaller than 100 nm (purple, dotted) and 50 nm (orange, dashed).

is the angle between the photon and electron momenta at the point of emission. We calculate L_f for each simulated photon, using $L_f \simeq r_c \vartheta$, where $r_c \simeq \gamma^2 / (m\chi_e)$ is the electron's instantaneous radius of curvature. Photons with formation lengths above a threshold value are then discarded in order to estimate the importance of nonlocal effects. As interference effects do not, in reality, completely suppress emission, this scheme tends to overestimate the necessary correction [43].

What value the maximum formation length L_f^{max} should take depends on the scenario in question. In the present case, we use the fact that the skin depth, the length over which the incident electromagnetic fields decay at the plasma surface, shown in the inset of fig. 1(a), is approximately $\lambda_p \simeq 100$ nm. Photons are emitted primarily at large polar angles $\cos \theta \simeq \beta_{\text{hb}}$ to the laser axis, where β_{hb} is the hole-boring velocity: thus an appropriate threshold would be $L_f^{\text{max}} \simeq \lambda_p / \beta_{\text{hb}} \simeq 240$ nm (recall $\beta_{\text{hb}} \simeq 0.40$ for a carbon plasma with density $n_e = 100n_{\text{cr}}$). Figure 4 shows the photon spectra (spontaneous, i.e. synchrotron emission only) from the simulations for three different values of L_f^{max} . We see that excluding all photons with formation lengths greater than 100 nm, or even 50 nm, has a small overall effect on the spectrum in the few-keV range. As photons must be emitted in order to be absorbed, or to stimulate further synchrotron emission, we

conclude that the LCFA is a reasonable approximation for the interaction studied in this work.

- [1] A. K. Harding and D. Lai, Physics of strongly magnetized neutron stars, [Rep. Prog. Phys. **69**, 2631 \(2006\)](#).
- [2] C. N. Danson, C. Haefner, J. Bromage, T. Butcher, J.-C. F. Chanteloup, E. A. Chowdhury, A. Galvanauskas, L. A. Gizzi, H. J., D. I. Hillier, N. W. Hopps, Y. Kato, E. A. Khazanov, R. Kodama, K. G., R. Li, Y. Li, J. Limpert, J. Ma, C. H. Nam, D. Neely, D. Papadopoulos, R. R. Penman, L. Qian, J. J. Rocca, A. A. Shaykin, C. W. Siders, C. Spindloe, S. Szatmári, R. M. G. M. Trines, J. Zhu, Z. P., and J. D. Zuegel, Petawatt and exawatt lasers worldwide, [High Power Laser Science and Engineering **7**, e54 \(2019\)](#).
- [3] T. Erber, High-energy electromagnetic conversion processes in intense magnetic fields, [Rev. Mod. Phys. **38**, 626 \(1966\)](#).
- [4] M. Marklund and P. K. Shukla, Nonlinear collective effects in photon-photon and photon-plasma interactions, [Rev. Mod. Phys. **78**, 591 \(2006\)](#).
- [5] A. Di Piazza, C. Müller, K. Z. Hatsagortsyan, and C. H. Keitel, Extremely high-intensity laser interactions with fundamental quantum systems, [Rev. Mod. Phys. **84**, 1177 \(2012\)](#).
- [6] D. Papadopoulos, J. Zou, C. Le Blanc, G. Chériaux, P. Georges, F. Druon, G. Mennerat, P. Ramirez, L. Martin, A. Fréneaux, A. Beluze, N. Lebas, P. Monot, F. Mathieu, and P. Audebert, The Apollon 10 PW laser: experimental and theoretical investigation of the temporal characteristics, [High Power Laser Science and Engineering **4**, e34 \(2016\)](#).
- [7] S. Weber, S. Bechet, S. Borneis, L. Brabec, M. Bučka, E. Chacon-Golcher, M. Ciappina, M. DeMarco, A. Fajstavr, K. Falk, E.-R. Garcia, J. Grosz, Y.-J. Gu, J.-C. Hernandez, M. Holec, P. Janečka, M. Jantač, M. Jirka, H. Kadlecova, D. Khikhlikha, O. Klimo, G. Korn, D. Kramer, D. Kumar, T. Lastovička, P. Lutoslawski, L. Morejon, V. Olšovcová, M. Rajdl, O. Renner, B. Rus, S. Singh, M. Šmid, M. Sokol, R. Versaci, R. Vrána, M. Vranic, J. Vyskočil, A. Wolf, and Q. Yu, P3: An installation for high-energy density plasma physics and ultra-high intensity laser-matter interaction at ELI-Beamlines, [Matter and Radiation at Extremes **2**, 149 \(2017\)](#).
- [8] S. Gales, K. A. Tanaka, D. L. Balabanski, F. Negoita, D. Stutman, O. Tesileanu, C. A. Ur, D. Ursescu, I. Andrei, S. Ataman, M. O. Cernaianu, L. D'Alessi, I. Dancus, B. Diaconescu, N. Djourellov, D. F. Filipescu, P. Ghenuche, D. G. Ghita, C. Matei, K. Seto, M. Zeng, and N. V. Zamfir, The extreme light

- infrastructure–nuclear physics (ELI-NP) facility: new horizons in physics with 10 PW ultra-intense lasers and 20 MeV brilliant gamma beams, [Rep. Prog. Phys. **81**, 094301 \(2018\)](#).
- [9] R. E. Waltz and O. P. Manley, Synchrotron-like radiation from intense laser beams in dense plasmas, [The Physics of Fluids **21**, 808 \(1978\)](#).
- [10] C. P. Ridgers, C. S. Brady, R. Duclous, J. G. Kirk, K. Bennett, T. D. Arber, A. P. L. Robinson, and A. R. Bell, Dense electron-positron plasmas and ultraintense γ rays from laser-irradiated solids, [Phys. Rev. Lett. **108**, 165006 \(2012\)](#).
- [11] L. L. Ji, A. Pukhov, E. N. Nerush, I. Y. Kostyukov, B. F. Shen, and K. U. Akli, Energy partition, γ -ray emission, and radiation reaction in the near-quantum electrodynamical regime of laser-plasma interaction, [Phys. Plasmas **21**, 023109 \(2014\)](#).
- [12] E. N. Nerush and I. Y. Kostyukov, Laser-driven hole boring and gamma-ray emission in high-density plasmas, [Plasma Phys. Control. Fusion **57**, 035007 \(2015\)](#).
- [13] D. J. Stark, T. Toncian, and A. V. Arefiev, Enhanced multi-MeV photon emission by a laser-driven electron beam in a self-generated magnetic field, [Phys. Rev. Lett. **116**, 185003 \(2016\)](#).
- [14] C. P. Ridgers, J. G. Kirk, R. Duclous, T. G. Blackburn, C. S. Brady, K. Bennett, T. D. Arber, and A. R. Bell, Modelling gamma-ray photon emission and pair production in high-intensity laser-matter interactions, [J. Comp. Phys. **260**, 273 \(2014\)](#).
- [15] A. Gonoskov, S. Bastrakov, E. Efimenko, A. Ilderton, M. Marklund, I. Meyerov, A. Muraviev, A. Sergeev, I. Surmin, and E. Wallin, Extended particle-in-cell schemes for physics in ultrastrong laser fields: Review and developments, [Phys. Rev. E **92**, 023305 \(2015\)](#).
- [16] A. Ilderton, B. King, and A. J. MacLeod, Absorption cross section in an intense plane wave background, [Phys. Rev. D **100**, 076002 \(2019\)](#).
- [17] A. I. Voroshilo, E. A. Padusenko, and S. P. Roshchupkin, One-photon annihilation of an electron-positron pair in the field of pulsed circularly polarized light wave, [Laser Phys. **20**, 1679 \(2010\)](#).
- [18] S. Tang, A. Ilderton, and B. King, One-photon pair annihilation in pulsed plane-wave backgrounds, [Phys. Rev. A **100**, 062119 \(2019\)](#).
- [19] M. S. Longair, *High Energy Astrophysics*, 3rd ed. (Cambridge University Press, 2011).
- [20] R. A. Chevalier, Synchrotron self-absorption in radio supernovae, [Astrophys. J. **499**, 810 \(1998\)](#).
- [21] J. Granot, T. Piran, and R. Sari, Synchrotron self-absorption in gamma-ray burst afterglow, [Astrophys. J. **527**, 236 \(1999\)](#).
- [22] T. Piran, The physics of gamma-ray bursts, [Rev. Mod. Phys. **76**, 1143 \(2005\)](#).

- [23] R. Fender and J. Bright, Synchrotron self-absorption and the minimum energy of optically thick radio flares from stellar mass black holes, [Mon. Not. R. Astron. Soc. **489**, 4836 \(2019\)](#).
- [24] D. B. Melrose, *Quantum Plasmadynamics: Unmagnetized Plasmas* (Springer, New York, 2008).
- [25] W. Heisenberg and H. Euler, Folgerungen aus der Diracschen Theorie des Positrons, [Z. Phys. **98**, 714 \(1936\)](#).
- [26] J. Schwinger, On gauge invariance and vacuum polarization, [Phys. Rev. **82**, 664 \(1951\)](#).
- [27] V. N. Baier, V. M. Katkov, and V. M. Strakhovenko, *Electromagnetic Processes at High Energies in Oriented Single Crystals* (World Scientific, Singapore, 1998).
- [28] G. Ghisellini and R. Svensson, The synchrotron and cyclo-synchrotron absorption cross-section, [Mon. Not. R. Astron. Soc. **252**, 313 \(1991\)](#).
- [29] V. I. Ritus, Quantum effects of the interaction of elementary particles with an intense electromagnetic field, [J. Sov. Laser Res. **6**, 497 \(1985\)](#).
- [30] C. N. Harvey, A. Ilderton, and B. King, Testing numerical implementations of strong-field electrodynamics, [Phys. Rev. A **91**, 013822 \(2015\)](#).
- [31] V. Dinu, C. Harvey, A. Ilderton, M. Marklund, and G. Torgrimsson, Quantum radiation reaction: From interference to incoherence, [Phys. Rev. Lett. **116**, 044801 \(2016\)](#).
- [32] A. Di Piazza, M. Tamburini, S. Meuren, and C. H. Keitel, Implementing nonlinear Compton scattering beyond the local-constant-field approximation, [Phys. Rev. A **98**, 012134 \(2018\)](#).
- [33] T. G. Blackburn, D. Seipt, S. S. Bulanov, and M. Marklund, Benchmarking semiclassical approaches to strong-field QED: Nonlinear Compton scattering in intense laser pulses, [Phys. Plasmas **25**, 083108 \(2018\)](#).
- [34] A. Ilderton, B. King, and D. Seipt, Extended locally constant field approximation for nonlinear Compton scattering, [Phys. Rev. A **99**, 042121 \(2019\)](#).
- [35] B. King, Uniform locally constant field approximation for photon-seeded pair production, [Phys. Rev. A **101**, 042508 \(2020\)](#).
- [36] V. P. Oleinik, Resonance effects in the field of an intense laser beam, *Sov. Phys. JETP* **25**, 697 (1967).
- [37] J. Bergou, S. Varro, and M. V. Fedorov, e - e scattering in the presence of an external field, [J. Phys. A **14**, 2305 \(1981\)](#).
- [38] S. P. Roshchupkin, Resonant effects in collisions of relativistic electrons in the field of a light wave, *Laser Phys.* **6**, 837 (1996).
- [39] P. Panek, J. Z. Kamiński, and F. Ehlotzky, Analysis of resonances in Møller scattering in a laser field

- of relativistic radiation power, *Phys. Rev. A* **69**, 013404 (2004).
- [40] V. N. Nedoreshta, S. P. Roshchupkin, and A. I. Voroshilo, Resonance of the exchange amplitude of a photon by an electron scattering in a pulsed laser field, *Phys. Rev. A* **91**, 062110 (2015).
- [41] D. B. Melrose, Covariant form for the collision integral, *J. Plasma Phys.* **73**, 599 (2007).
- [42] E. G. Gamaliy and R. Dragila, Interaction of ultrashort laser pulses at relativistic intensities with solid targets: Relativistic skin effect, *Phys. Rev. A* **42**, 929 (1990).
- [43] T. G. Blackburn, D. Seipt, S. S. Bulanov, and M. Marklund, Radiation beaming in the quantum regime, *Phys. Rev. A* **101**, 012505 (2020).
- [44] K. Nanbu and S. Yonemura, Weighted particles in Coulomb collision simulations based on the theory of a cumulative scattering, *J. Comput. Phys.* **145**, 639 (1998).
- [45] Y. Sentoku and A. J. Kemp, Numerical methods for particle simulations at extreme densities and temperatures: Weighted particles, relativistic collisions and reduced currents, *J. Comput. Phys.* **227**, 6846 (2008).
- [46] F. Del Gaudio, T. Grismayer, R. A. Fonseca, and L. O. Silva, Compton scattering in particle-in-cell codes, *J. Plasma Phys.* **86**, 905860516 (2020).
- [47] A. P. L. Robinson, P. Gibbon, M. Zepf, S. Kar, R. G. Evans, and C. Bellei, Relativistically correct hole-boring and ion acceleration by circularly polarized laser pulses, *Plasma Phys. Control. Fusion* **51**, 024004 (2009).
- [48] T. G. Blackburn, OPAL, <https://github.com/tgblackburn/opal> (2020).
- [49] T. G. Blackburn, Self-absorption of synchrotron radiation in a laser-irradiated plasma, Zenodo. <https://doi.org/10.5281/zenodo.3993062> (2020).